Earthquakes and Structures, *Vol. 16, No. 2 (2019) 209-219*
DOI: https://doi.org/10.12989/eas.2019.16.2.209

Snap back testing of unbonded post-tensioned concrete wall systems

Kimberley M. Twigden[1] and Richard S. Henry[*2]

[1]*Aurecon, PO Box 9762, Newmarket, Auckland, 1149, New Zealand*
[2]*Dept. of Civil and Environmental Engineering, University of Auckland, Auckland, 1010, New Zealand*

(Received April 28, 2018, Revised November 16, 2018, Accepted January 16, 2019)

Abstract. Unbonded Post-Tensioned (UPT) precast concrete systems have been shown to provide excellent seismic resistance. In order to improve understanding of the dynamic response of UPT systems, a series of snap back tests on four UPT systems was undertaken consisting of one Single Rocking Wall (SRW) and three Precast Wall with End Columns (PreWEC) systems. The snap back tests provided both a static pushover and a nonlinear free vibration response of a system. As expected the SRW exhibited an approximate bi-linear inertia force-drift response during the free vibration decay and the PreWEC walls showed an inertia force-drift response with increased strength and energy dissipation due to the addition of steel O-connectors. All walls exhibited negligible residual drifts regardless of the number of O-connectors or the post-tensioning force. When PreWEC systems of the same strength were compared the inclusion of further energy dissipating O-connectors was found to decrease the measured peak wall acceleration. Both the local and global wall parameters measured at pseudo-static and dynamic loading rates showed similar behaviour, which demonstrates that the dynamic behaviour of UPT walls is well represented by pseudo-static tests. The SRW was found to have Equivalent Viscous Damping (EVD) between 0.9-3.8% and the three PreWEC walls were found to have maximum EVD of between 14.7-25.8%.

Keywords: self-centering; unbonded post-tensioning; precast concrete; shear wall; dynamic loading; PreWEC; O-connector; energy dissipation

1. Introduction

The concept of low-damage seismic resisting systems that utilise Unbonded Post-Tensioning (UPT) is well developed (Kurama *et al*. 2018). The simplest form of a UPT wall system consists of a single precast concrete panel connected to the foundation using UPT tendons, referred to herein as a Single Rocking Wall (SRW). Due to the concentration of deformations at the base of the SRW, the lateral load response is essentially non-linear elastic and so additional energy dissipating elements are often used to increase the energy dissipation capability of UPT wall systems. Examples of such wall systems include hybrid walls that use additional mild steel bars placed at the wall-foundation interface (Holden *et al*. 2003, Kurama 2002) and jointed wall systems consists of two or more panels connected vertically by energy dissipating connectors (Galusha 1999, Priestley *et al*. 1999). A new UPT wall system with additional energy dissipating elements has recently been developed that consists of a Precast Wall with End Columns (PreWEC) (Sritharan *et al*. 2015). The PreWEC system consists of a SRW connected vertically to two Post-Tensioned (PT) end columns using specially designed energy dissipating connectors termed O-connectors (Henry *et al*. 2010). The PreWEC system has a significant advantage over jointed wall systems due to the column-wall-column arrangement that maximises the lateral load capacity and provides an innovative method to attach the floors where the end columns support gravity demands and the wall panel is free to uplift vertically relative to the floor (Henry *et al*. 2016).

UPT wall systems have been subject to numerous pseudo-static lateral load tests (Henry *et al*. 2012, Holden *et al*. 2003, Perez *et al*. 2013, Sritharan *et al*. 2015). However, only a limited number of experiments have been conducted to investigate the dynamic response of UPT walls. Wight *et al*. (2006) performed shake table tests on a masonry UPT system, Marriott *et al*. (2008) performed shake table testing on hybrid systems with various combinations of viscous dampers and mild steel yielding fuses, and Nazari *et al*. (2017) preformed shake-table tests of a series of SRWs. Shake table tests have also been conducted on large scale building assemblies as reported by Belleri *et al*. (2014) at University of California San Diego and at the E-defense laboratory in Japan (Nagae *et al*. 2014). Both of these large-scale tests incorporated hybrid walls similar to those investigated by Marriott *et al*. (2008).

Due to the lack of dynamic testing on vertically jointed UPT wall systems such as the PreWEC system, the dynamic behaviour and hence seismic performance of such UPT systems is not fully understood. In an effort to fill this knowledge gap a series of snap back tests on one SRW and three PreWEC systems was undertaken. Snap back testing is advantageous as it provides both the static and dynamic response of a system consisting of both the pseudo-static pushover and subsequent free vibration response. The objective of the snap back tests was to systematically investigate the dynamic characteristics of UPT wall systems

*Corresponding author, Ph.D.
E-mail: rs.henry@auckland.ac.nz

ISSN: 2092-7614 (Print), 2092-7622 (Online)

Table 1 Wall specifications

Wall Label	Tendon #	f_{pi} (MPa)		f'_c (MPa)	f'_g (MPa)	AFR (f_c/f'_c) (%)		O-connectors per joint
		Target	Achieved			Target	Achieved	
SRW-A	3	696	714	34.8	57.5	7.5	9.9	-
PreWEC-A	3	696	696	35.8	61.4	7.5	9.4	4
PreWEC-B	3	696	699	42.4	39.6	7.5	8.0	6
PreWEC-C	2	696	762	37.4	59.5	5	6.8	6

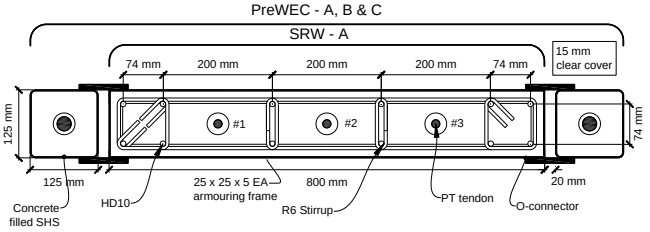

Fig. 1 Wall cross section detail

and to provide comparisons of response parameters evaluated at both pseudo-static and dynamic loading rates. Previously performed pseudo-static cyclic tests on identical walls (Twigden *et al*. 2017) provided a valuable comparison with the dynamic force-displacement measurements and Equivalent Viscous Damping (EVD) estimates.

2. Test walls

The experimental programme consisted of snap back tests on four walls, including one SRW (SRW-A) and three PreWEC systems (PreWEC-A, B, and C). The three PreWEC walls had identical dimensions and material properties, but the initial PT force and number of O-connectors was varied. Test walls SRW-A, PreWEC-A, and B had the same dimensions and parameters as three walls subjected to pseudo-static cyclic testing reported elsewhere (Twigden *et al*. 2017). The specimen dimensions and parameters were selected to represent a four-storey prototype building at 1/5th scale as described in detail in Twigden (2015). The test results presented are discussed for the as-built wall specimens.

2.1 Wall specifications

The dimensions, design parameters, and cross section of each test wall are provided in Fig. 1 and Table 1. Identical precast concrete wall panels were used for each wall system that were 800 mm long, 125 mm thick, and 2860 mm high, respectively, and cast with ducts along the length for placement of the UPT tendons. Test walls SRW-A, PreWEC-A, and B, each used three tendons and PreWEC-C used only two tendons. The PT tendons consisted of a single 15.2 mm prestressing strand with an unbonded length of 3600 mm and a targeted initial prestress (f_{pi}) of 696 MPa ($0.45f_y$). The targeted prestress force was selected to maximise the wall moment capacity while keeping the Axial Force Ratio (AFR) below 10% to ensure that no significant crushing occurred in the wall compression toe. As shown in Table 1, the AFRs calculated from the measured material properties and tension forces for walls SRW-A, PreWEC-A, B, and C were 9.9%, 9.4 %, 8.0%, and 6.8% respectively. In addition, the tendon configuration and initial prestress were designed to ensure that the tendon force did not exceed the yield strength of the strand until lateral drifts of over 3% were reached.

Horizontal reinforcement consisted of 6 mm diameter bars at 100 mm centres was used for the panel in combination with minimum vertical reinforcement that consisted of 12-HD10 bars and the wall toes consisted of confinement reinforcement in the form of 6 mm diameter closed stirrups spaced vertically at 40 mm centres, as detailed in Fig. 1. The confinement reinforcement was designed for the wall toe using the confined concrete model described by Mander *et al*. (1998), to sustain a maximum expected compressive strain in the wall toe calculated using the simplified analysis method proposed by Aaleti and Sritharan (2009). A steel angle base frame constructed from 25×25×5 mm equal angle was cast into the end of each precast wall for additional confinement and protection of the panel edge, as shown and discussed in Twigden *et al* (2017).

PreWEC-A, B, and C consisted of identical wall panels to SRW-A with the addition of two UPT end columns constructed from concrete filled 125×125×5 mm square steel hollow sections (SHS). The targeted initial PT force of the end columns was 220 kN per column, using a 26.5 mm diameter stress-bar with an unbonded length of 3000 mm for all PreWEC tests. The targeted initial PT force in the columns was selected to ensure that the columns did not lift off the foundation using the Aaleti and Sritharan (2009) design procedure. The energy dissipating O-connectors were placed across the wall-to-column joint, welded between the SHS and steel plates that were embedded into the wall panel. As presented in Table 1, PreWEC-A, B, and C were designed to have 4,6 and 6 O-connectors per joint, respectively, creating three systems with different quantities of hysteretic energy dissipation and varying flexural capacities that can be described by moment contributions ratios (λ) of 3.25, 2.3, and 2.0 for a design drift of 1.2%. The moment contribution ratio is the ratio of the flexural capacity provided by the PT and axial load to that provided by the hysteretic dissipating devices (as defined in Appendix B of NZS 3101:2006).

2.2 Material properties

Test cylinders and cubes were used to determine the compressive strength of the wall panel concrete and wall base grout respectively. The measured concrete (f'_c) and grout (f'_g) strengths on the day of testing for each wall are

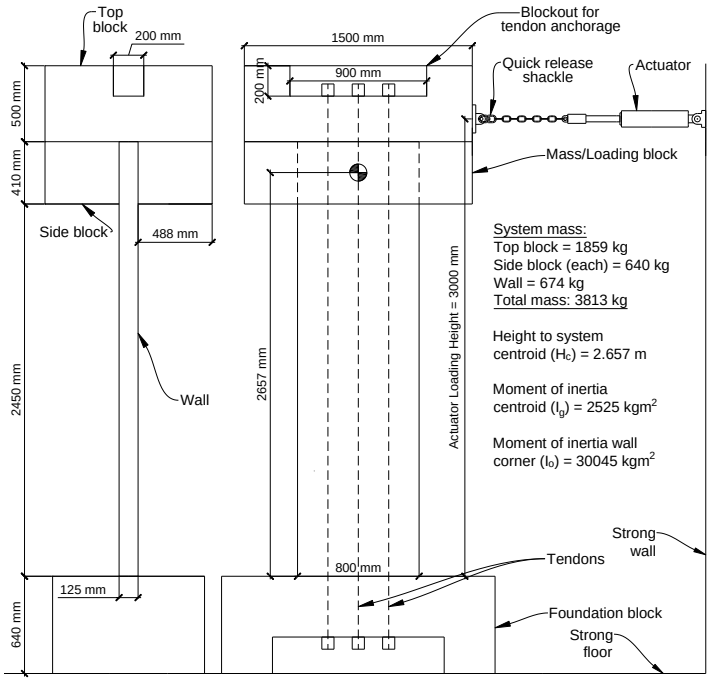

(a) Geometry (SRW)

(b) PreWEC-A

Fig. 2 Snap back test setup

provided in Table 1. Three tensile tests of the 15.2 mm strand were conducted and the measured properties included a proof yield strength of 1540 MPa, a modulus of elasticity of 199.5 MPa, and an ultimate strength of 1735 MPa. The ultimate strength was lower than the 1825 MPa stated on the mill test certificate due to premature fracture of strand close to the anchorage at elongations of approximately 1%, which has been found to be a common problem with existing monostrand anchors (Walsh and Kurama 2010), and new anchorage systems have been developed to overcome this issue (Abramson 2013). The premature strand failure was not considered critical as the initial PT was selected to prevent the strand exceeding the yield strain during testing. The 26.5 mm stress-bar had a nominal ultimate tensile strength of 1030 MPa and a nominal 0.1% proof stress of 835 MPa. The concrete filled SHS used for the end columns had a concrete compressive strength of 38.2 MPa determined on the day of testing of the first PreWEC wall. The properties of the wall vertical and horizontal reinforcement are not critical to the test results, but are identical to those already reported by Twigden *et al* (2017).

2.3 O-connector properties

The O-connectors used for this experimental programme were laser cut from 10 mm thick mild steel plate, with the geometry shown in Fig. 3. The material properties of the mild steel plate established from uniaxial tension tests included a yield strength of 317 MPa, ultimate strength of 522 MPa, modulus of elasticity of 201.5 GPa and ultimate elongation of 24.9 %. Additional details and component test results of the O-connectors used are reported in Twigden and Henry (2015), where the geometry type "O1" are

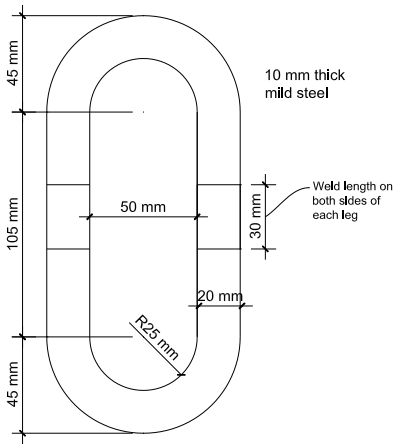

Fig. 3 O-connector geometry

identical to the connectors used during the wall snap back tests.

3. Test setup

A schematic of the SRW-A geometry and test setup is presented in Fig. 2(a). The typical PreWEC system test setup was identical except for the inclusion of the end columns and O-connectors, as shown in the photo in Fig. 2(b). The wall panel in each test was seated in a shallow pocket on top of the foundation that was filled with grout to provide an even bearing surface at the wall-to-foundation interface. The wall panel was embedded approximately 10 mm into the grout pocket to increase the sliding shear resistance. To limit the concrete compressive strains and spalling of cover concrete in the toe region, each wall panel

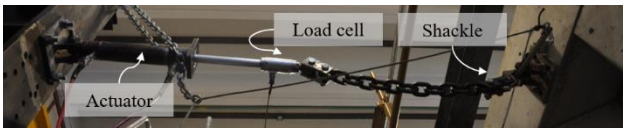

Fig. 4 Snap back test load application rig

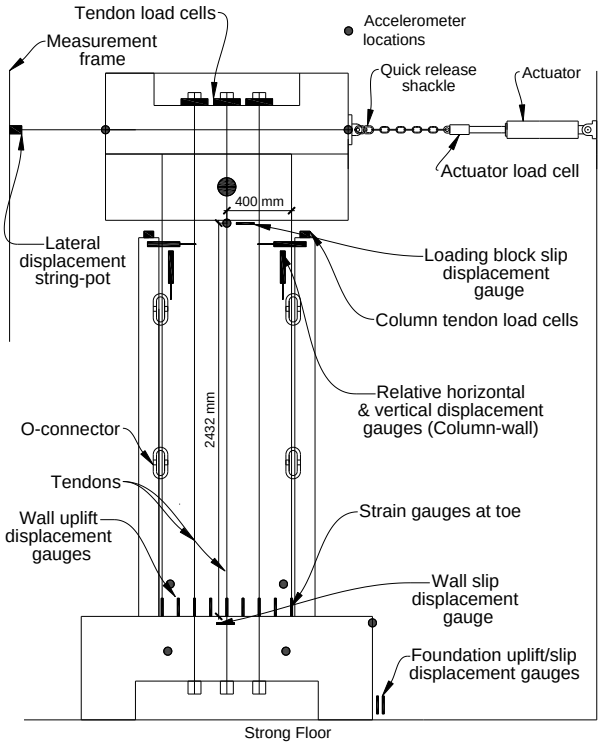

Fig. 5 Instrumentation

had a foam strip glued across the wall thickness in the corner of each wall for the width of the cover region (15 mm). Use of the foam strip effectively shortened the length of the wall by 30 mm to 770 mm. Concrete mass blocks were attached to the top of the wall providing anchorage for the tendons, seismic mass for the dynamic testing, and a loading beam for the load application snap back test rig. A photo of the lateral load application and release rig used for the snap back testing is shown in Fig. 4. The rig consisted of a hydraulic jack and load cell connected by a heavy-duty chain to a quick release mechanism. The quick release mechanism was a shackle that could be remotely triggered to open when under load. A steel lateral support frame provided out-of-plane restraint to the wall during testing. The total mass of the wall and additional weight was 3813 kg with a centre of mass of 2.657 m above the wall base.

Extensive instrumentation was installed on all walls to capture both the pseudo-static pull-back and free-vibration response, with the typical sensor layout shown in Fig. 5. Displacement gauges were used to measure wall lateral displacement, wall uplift, and potential slip at the wall-foundation interface, wall-anchorage block interface, and the foundation to strong floor interface. Strain gauges were also placed at the wall toes to capture the peak compressive strains. Load cells were used to measure and apply the tendon forces in the wall and columns, as well as to measure the lateral load applied during the pull-back phase of the snap test. For each PreWEC test, displacement gauges were also used to measure the relative vertical and horizontal displacement along each column-wall joint to capture the displacements applied to the O-connectors. An array of accelerometers was used to measure in-plane, out-of-plane, and vertical accelerations at several locations on the test setup. The data acquisition system recorded at a sampling rate of 2000 Hz. All of the dynamic test data reported has been filtered with a 30 Hz low pass filter to remove any high frequency noise from the data acquisition system unless otherwise stated, and all lateral motion results are reported at the height of the Centre of Mass (CoM).

4. Test procedure

In addition to the main snap-back tests, small vibration tests were also performed on each wall by striking the top of the wall with an impact hammer to identify the fundamental natural frequency of each wall system. The snap back tests were then conducted by pulling the wall back to a specified lateral drift and activating the quick release mechanism, allowing the wall to vibrate freely until rest. Each wall was subjected to snap back tests from lateral drifts of 1% and 2%. These drifts correspond to typical design level drifts for concrete wall systems and were sufficient to induce rocking and nonlinear response that would be expected to occur during a design level earthquake.

5. Test results and discussion

5.1 Frequency characterisation and stiffness

The natural frequencies of the four test walls were calculated by applying a fast Fourier transform to the recorded acceleration data at the top of the wall during impact hammer excitations. SRW-A was found to have a fundamental frequency of 8.2 Hz and the three PreWEC walls had the same fundamental frequency of 10.6 Hz. As expected from the design, the PreWEC systems had a higher stiffness than SRW-A due to the contribution of the O-connectors and end columns. However, the number of O-connectors connecting the columns did not significantly affect the initial stiffness of the PreWEC systems, indicating that the effect of the coupling between the wall and columns was equivalent regardless of number of O-connectors.

During the hammer hits no uplift occurred at the wall base which implied that the theoretical lateral stiffness should be calculated based on the uncracked gross section moment of inertia (I_g). A prediction of the initial stiffness ($K_{i(p)}$) was calculated assuming a lateral stiffness (K) equal to the sum of $3EI_g/h^3$ for each component (walls and columns), where E is the modulus of elasticity, I_g the moment of inertia and h the height of the applied load (CoM for dynamic loading (Chopra 2007)). The calculation assumed a concrete modulus of elasticity (E_c) equal to $4700\sqrt{f_c'}$, where f_c' is the compressive strength of concrete in MPa. A measured initial stiffness ($K_{i(m)}$) was

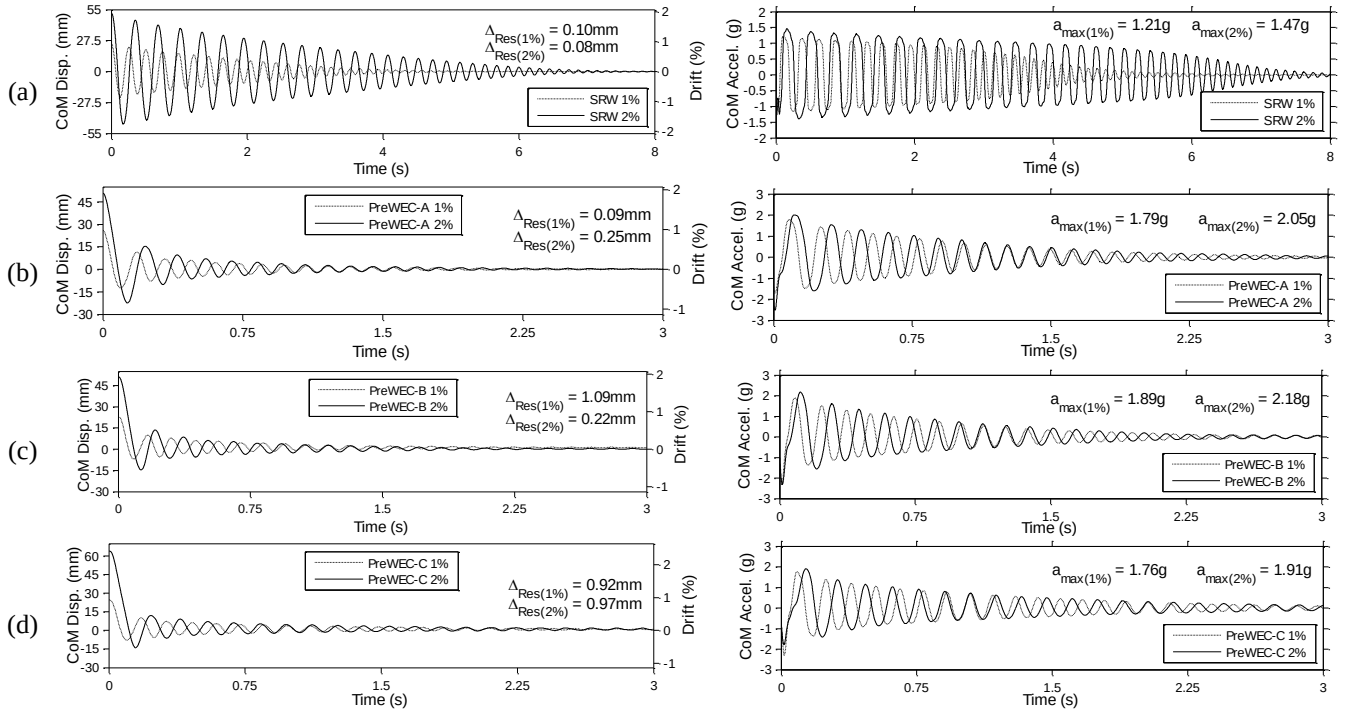

Fig. 6 Displacement and acceleration decay (a) SRW-A, (b) PreWEC-A, (c) PreWEC-B, (d) PreWEC-C

Table 2 Initial stiffness of each test specimen

Ki (kN/mm)	SRW-A	PreWEC-A	PreWEC-B	PreWEC-C
Measured	10.4	17.3	17.3	17.3
Predicted	21.1	21.6	23.5	22.1
Measured/ Predicted	0.49	0.80	0.74	0.78

derived from the measured fundamental frequency using a mass of 3813 kg. The measured stiffness of SRW-A was 10.4 kN/mm, and 17.3 kN/mm for all PreWEC walls. The predicted and measured initial stiffness for each wall is presented in Table 2 alongside an Effective Stiffness Modifier (ESM) which is equal to the measured stiffness divided by the predicted stiffness. For SRW-A the ESM was 0.49 and ranged between 0.74-0.8 for the PreWEC systems, demonstrating that use of the gross section properties significantly overestimates the stiffness. The effective stiffness modifier values aligned well with previous values calculated from the initial cycles during pseudo-static cyclic testing (Twigden *et al*. 2017).

5.2 Observations and time history response

The SRW-A displacement and acceleration decays during snap back tests to both 1% and 2% lateral drift are presented in Fig. 6(a). Both snap back tests resulted in large amplitude rocking that lasted up to 8s for the 2% drift test. The decay envelope was noticeably more linear in profile than the exponential envelope expected for a viscous system. During each of the tests, no significant damage was observed in the wall panel toes, as demonstrated by the photo of the wall base after the snap back tests in Fig. 7(a).

The displacement and acceleration decays for snap back tests from 1% and 2% lateral drift for PreWEC-A, B and C

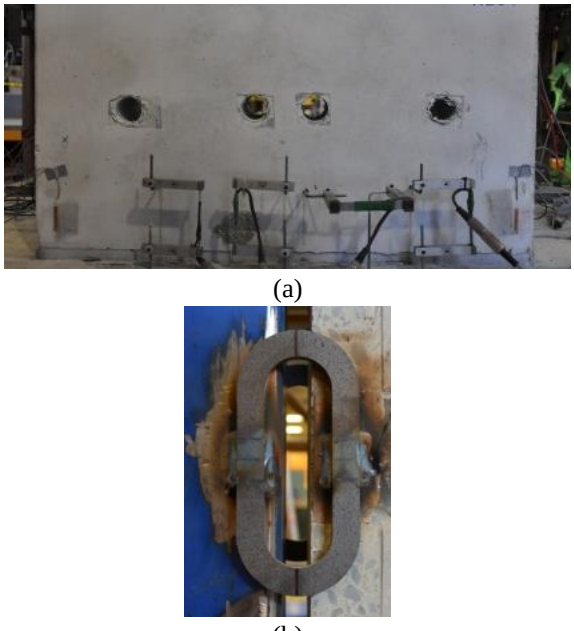

(a)

(b)

Fig. 7 Examples of post-test condition (a) SRW-A (b) O-connector (PreWEC-A)

are presented in Fig. 6(b), (c), and (d), respectively. Each of the PreWEC systems exhibited noticeable rocking at the wall base for only two to three cycles and each of the systems vibration lasted approximately 3s. The decay envelope of the PreWEC systems displacement response was more exponential in shape compared to that for SRW-A. The snap back tests performed on the three PreWEC walls also resulted in negligible damage to the wall panels and the O-connector displacements were within their design range, with no connector failure during any of the tests. An

Table 3 Wall peak accelerations and residual drifts

Wall	Peak acceleration (g)		Residual drift (%)	
	1% snap back	2% snap back	1% snap back	2% snap back
SRW-A	1.21	1.47	0.0038	0.0030
PreWEC-A	1.79	2.05	0.0034	0.0083
PreWEC-B	1.89	2.18	0.0094	0.035
PreWEC-C	1.76	1.91	0.041	0.037

example of the O-connector condition after the PreWEC-A snap back tests is shown in Fig. 7(b).

The recorded peak accelerations (α_{max} in the acceleration plots) following release (ignoring the impulse at the start of the decay) for both the 1% and 2% drift tests are shown in Table 3. All of the PreWEC systems had measured peak accelerations higher than that of SRW-A due to the higher moment capacity of the systems. In addition, the peak accelerations of PreWEC-C were less than that of PreWEC-A despite them being designed to have comparable moment capacity. This result confirmed that the increased hysteretic energy dissipation from the additional O-connectors in PreWEC-C resulted in reduced peak accelerations.

5.3 Residual drifts

All the walls returned to their original vertical alignment with negligible residual drift at the conclusion of the snap back tests. The measured residual displacements (Δ_{Res}) are shown within each displacement decay plot in Fig. 6 and the residual drifts can be calculated by dividing the residual displacement by the height to the CoM (2657 mm), as summarised in Table 3. In general, the PreWEC systems had higher residual drifts than SRW-A, but never of a magnitude higher than 0.04%. The measured residual drift following snap back tests were significantly less than the respective residual drifts measured during pseudo-static cyclic testing of identical walls (Twigden *et al*. 2017). This finding highlights the importance of the dynamic response and decay on residual drifts. Although the snap back tests do not simulate earthquake excitation, the snap back tests still provide evidence for the tendency of the system to self-centre during the free vibration phase at the end of a ground motion. The significant difference between the residual drift observed in the cyclic hysteresis response of the test walls and the residual drift observed during dynamic free vibration decay is in agreement with previous analytical research (Henry *et al*. 2016) that predicted lower dynamic residual drifts than static residual drifts. Additionally, it is worth noting that negligible slip was measured at the wall base for all test walls during all test types

5.4 Lateral force displacement behaviour

The static monotonic moment-drift response was also measured when the wall was initially displaced. For all wall configurations, the measured monotonic moment drift responses for pull-backs to 1% and 2% drift are presented in Fig. 8(a) and (b), respectively. As expected the PreWEC systems showed higher moment capacities than SRW-A due

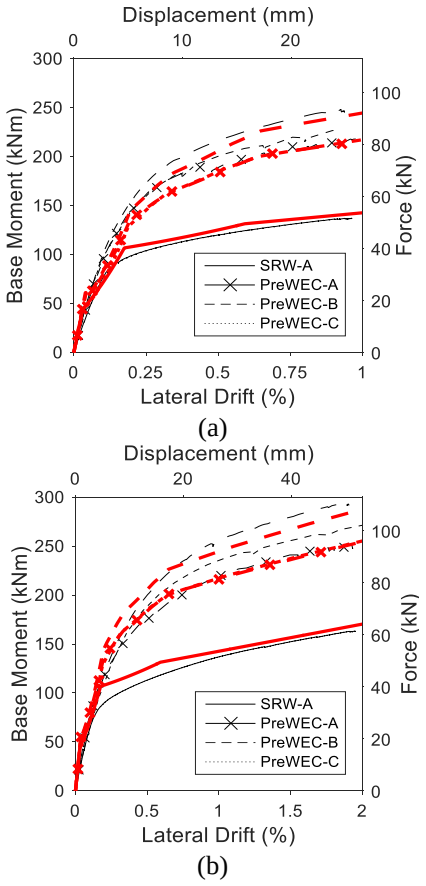

Fig. 8 Monotonic moment drift results (a) 1% and (b) 2%

to the addition of O-connectors. Although PreWEC-A and C were designed to have a similar moment drift response by decreasing the wall PT force and increasing the number of O-connectors, a slightly higher moment capacity was measured for PreWEC-C. Also included in Fig. 8 is an analytical prediction of the moment-drift response of each wall system using the design procedure proposed by Aaleti and Sritharan (A&S) (2009). The analytical method is plotted in bold red with the corresponding pattern for each wall specified in the legend. The analytical predictions in red for PreWEC-A and PreWEC-C are almost identical and therefore overlaid on each other. The results of the A&S analytical method correlated well with the measured response for all four walls and is recommended for use in design of UPT concrete wall systems.

The dynamic force-displacement response of each test wall for both the 1% and 2% drift snap back tests is compared against the pseudo-static monotonic pull back and A&S prediction in Fig. 9. The dynamic force is the inertia force acting on the wall and was calculated by multiplying the total mass by the acceleration at the CoM. The inertia force displacement response of SRW-A exhibited an imperfect bilinear elastic response with a small amount of hysteresis. As expected the PreWEC walls exhibited fatter hysteresis loops with increased energy dissipation due to the addition of the O-connectors. For each wall the pull-back monotonic force-displacement response indicated some stiffness degradation in the system between the 1% and 2% drift tests due a small amount of

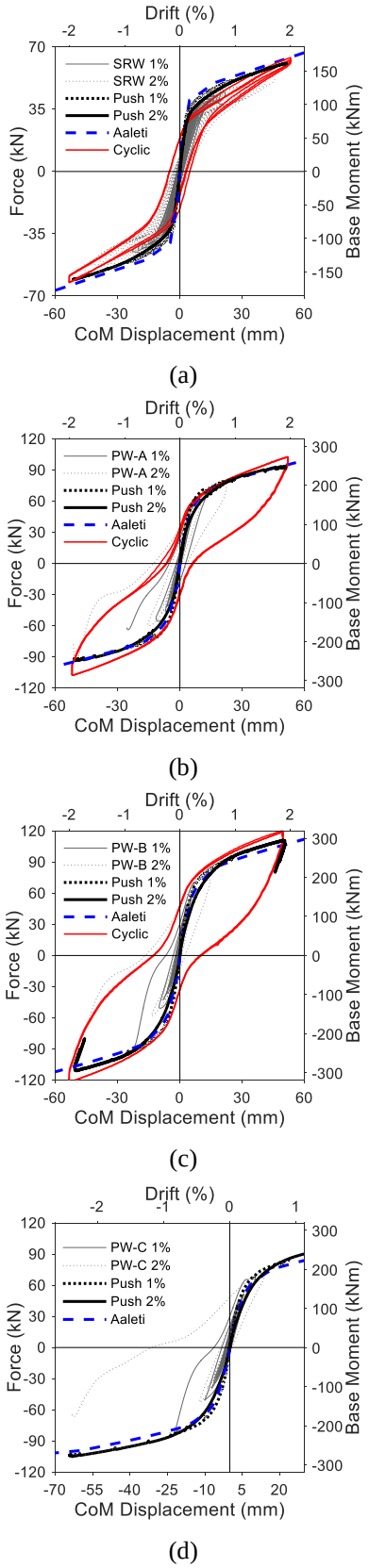

Fig. 9 Force-displacement response for (a) SRW-A, (b) PreWEC-A, (c) PreWEC-B, (d) PreWEC-C

PT loss and a small amount of inelastic concrete strain in the wall toes.

The pseudo-static cyclic force-displacement cycles for 2% lateral drift that were recorded during previous cyclic tests (Twigden *et al*. 2017) are also shown in Fig. 9. There is a close correlation between the pseudo-static cyclic results and the dynamic inertia force-displacement response measured during the snap back tests. The cyclic data indicated slightly higher strengths at large drifts, most likely due to the strain hardening effect on the O-connectors during cumulative reverse cyclic loading. The close alignment of the cyclic test, monotonic pull back, and inertia force during dynamic test responses demonstrates the consistency in behaviour of UPT walls regardless of loading rate.

6. Pseudo-static vs. dynamic test response

To investigate the change in local response parameters between pseudo-static and dynamic loading rates the neutral axis (NA), PT force, and compressive concrete toe strains for SRW-A and PreWEC-A are plotted in Fig. 10. The monotonic pushover (PO) measured during the pullback phase and free vibration decay (Decay) of the response are identified separately in each plot. PreWEC-A is used as an example for the PreWEC systems as similar local parameter responses were observed between the three test walls. The local response parameter results of all PreWEC systems can be found in Twigden (2015).

As shown in Fig. 10(a) and (b) for SRW-A and PreWEC-A, respectively, during each snap back tests pullback phase the PT force increased with increasing drift due to gap opening at the wall base. For the 1% drift SRW-A test it is clear when comparing the pushover PT response with the 1% decay PT response that a small amount of prestress loss resulted from the pushover phase, evidenced by the 1% decay path being lower than the initial prestress at zero drift. The prestress loss results from wedge draw-in as the force on the anchorage is increased, and since the PT force only decreases during the decay phase, no further loss developed during free vibration response. For SRW the 2% drift test pull back followed the same path as the 1% decay and prestress loss resulted again from the wedge draw-in that occurred during the pullback resulting in the 2% decay following a lower path. Similar behaviour to SRW-A was observed for PreWEC-A as shown in Fig. 10(b). Overall at the culmination of testing SRW-A had a total prestress loss of 5.2% and PreWEC-A had a prestress loss of 4.3%.

An example of the measured compressive strain in one of the wall toes when loaded in compression is plotted for SRW-A and PreWEC-A in Fig. 10(c), and (d), respectively. The exact location of the strain gauge is not significant, instead it is important to compare the strains measured in the same location during the tests at different loading rates. To assess the strain demand during the two different test phases, the pull-back response and free vibration are identified separately and only the peak strains in the compression toe at each displacement peak during the free vibration decay phase are plotted. For SRW-A the strains during the dynamic free vibration decay were higher than the pseudo-static pull back showing that the dynamic impact forces cause higher wall strains. However, for the

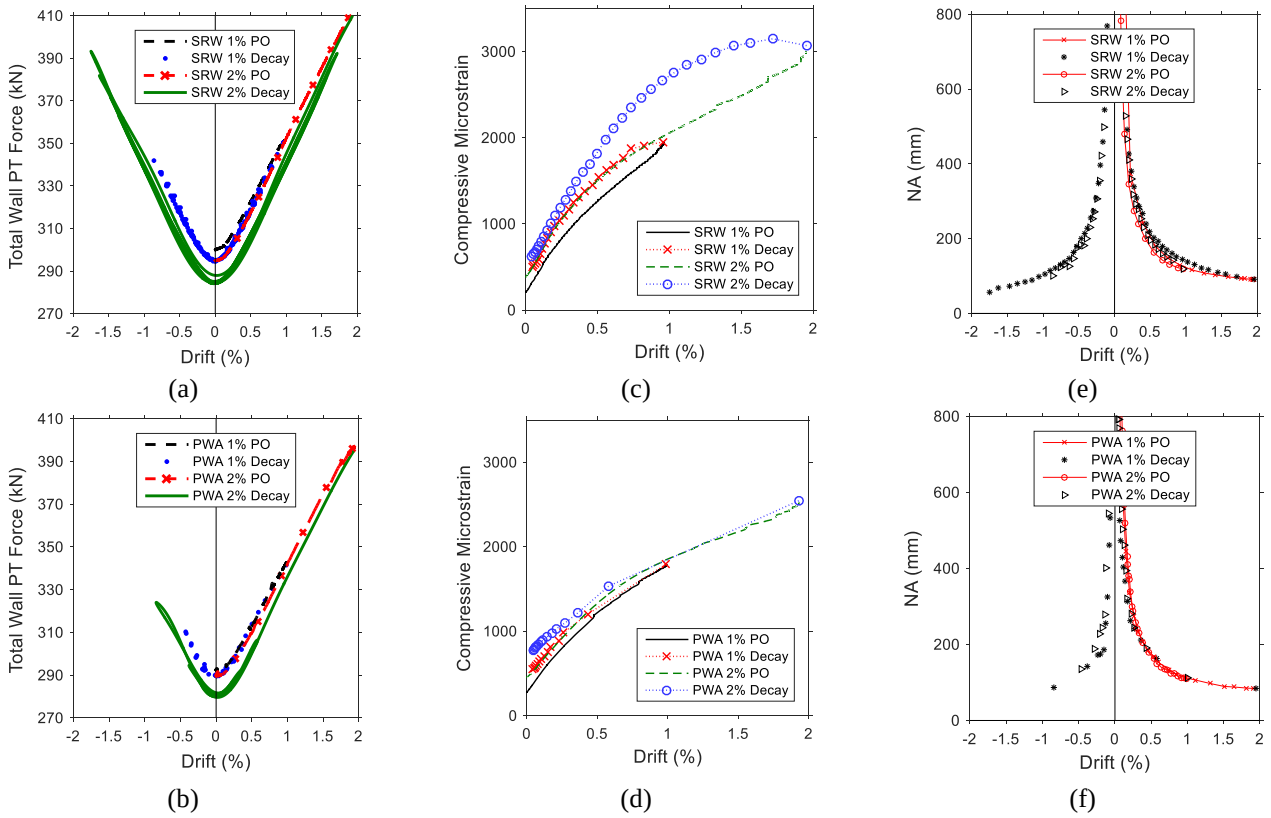

Fig. 10 Local wall parameter response versus drift (a) SRW-A PT, (b) PreWEC-A PT, (c) SRW-A strain, (d) PreWEC-A strain, (e) SRW-A NA, (f) PreWEC-A NA

three PreWEC systems (with PreWEC-A as an example) this pattern was not observed, likely due to the rapid decay of the walls resulting in no strain data points existing at drifts greater than 0.5% for the free vibration phase. It is expected that higher strains during the dynamic response would have occurred in the PreWEC walls if higher drifts were achieved during the rocking phase of the response. As demonstrated by Fig. 10(e), and (f), the NA for all walls during the pseudo-static and dynamic testing was in excellent agreement. The local parameters demonstrate that the dynamic behaviour of UPT wall systems can be well represented by pseudo-static tests for parameters such as NA and PT force, but higher strains can be expected due to toe impact during rocking.

7. Equivalent Viscous Damping (EVD)

7.1 Logarithmic decrement theory

A common method used to experimentally evaluate the EVD of linear structures is the Logarithmic Decrement Method (LDM) described by Eq. (1) (Chopra 2007), where u_n and u_{n+2} are a pair of positive or negative successive displacement peaks in the decay. Due to the amplitude dependence of the PT rocking system the classical equations for free vibration of a linear SDOF system are not strictly appropriate. However, the LDM is still often used for nonlinear structures as it is a simple technique to get an indication of the EVD appropriate to the system.

$$\delta = \ln\left(\frac{u_n}{u_{n+2}}\right) = \frac{2\pi\xi_{eq}}{\sqrt{1-\xi_{eq}^2}} \quad (1)$$

During an experimental free vibration decay small residual drifts may occur. Any residual drift will influence the EVD evaluated using the LDM, especially as the amplitude of displacement approaches the magnitude of residual drift. An Adjusted Logarithmic Decrement Method (ALDM) that accounts for residual drift is described by Eq. (2). The ALDM adjusts the pair of successive peaks used in Eq. (1) by replacing u_n with the absolute result of $u_n - u_{n+1}$, and u_{n+2} with the absolute result of $u_{n+1} - u_{n+2}$. The use of consecutive pairs of peaks effectively cancels out any residual drift that would affect the regular LDM. An example that demonstrates the validity of ALDM can be found in Twigden (2015).

$$\delta = \ln\left(\frac{abs(u_n - u_{n+1})}{abs(u_{n+1} - u_{n+2})}\right) = \frac{2\pi\xi_{eq}}{\sqrt{1-\xi_{eq}^2}} \quad (2)$$

As discussed previously the LDM uses the ratio of successive displacement peaks to determine an EVD ratio for linear systems assuming constant stiffness. For nonlinear systems the stiffness usually softens and the ratio of successive displacement peaks would tend to estimate EVD values that are too high. To better represent a nonlinear system Marriott (2009) showed that the square root of the initial input energy over the kinetic energy can be used in place of successive displacement peaks, as it can be proved for a linear system that the ratio of successive displacement peaks is equal to the square root of the ratio of

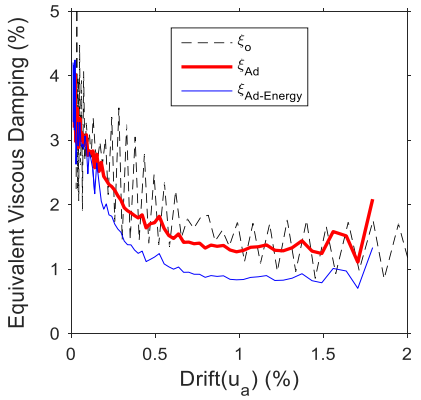

(a)

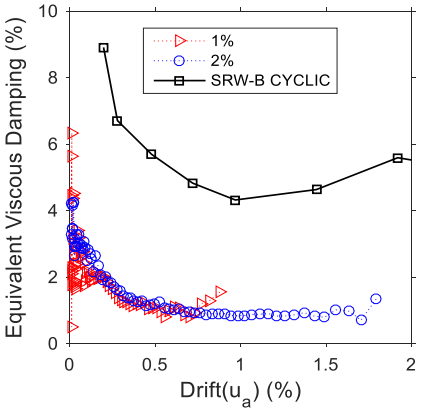

(b)

Fig. 11 SRW-A equivilent viscous damping, (a) 2% drift snap back, (b) comparison of snapback and cyclic tests

the total energy at the displacement peaks, as described by Eq. (3). For a nonlinear structure it is more appropriate to use the energy peaks as this takes the nonlinearity into account. Eq. (4) describes the logarithmic decrement method adjusted for residual drift and using total energy peaks in place of the successive displacement, referred to as the Adjusted Logarithmic Decrement Energy Method (ALDEM). When using ALDEM the total energy in a PT wall system at displacement peaks was assumed to be equal to the gravitational potential plus the total stored strain energy. The total strain energy was calculated using the peak displacement and the correlated amount of energy stored under the force-displacement loop. The gravitational potential energy was calculated as the total mass multiplied by gravity and the vertical displacement at the centre of the wall which was measured directly during the tests.

$$\frac{u_n}{u_{n+2}} = \sqrt{\frac{E_n}{E_{n+2}}} \tag{3}$$

$$\delta = \ln\left(\sqrt{\frac{abs(E_n - E_{n+1})}{abs(E_{n+1} - E_{n+2})}}\right) = \frac{2\pi\xi_{eq}}{\sqrt{1-\xi_{eq}^2}} \tag{4}$$

7.2 EVD test results

The EVD was evaluated for the 2% drift snap back test for SRW-A using the three methods described by Eqs. (1), (2), and (4), that correspond to the LDM (ξ_o), the ALDM (ξ_{Ad}), and the ALDEM ($\xi_{Ad-Energy}$). The calculated EVD for the three methods is plotted against the average of the drift peaks (u_a) in Fig. 11(a). It is particularly important to use the average of the drift peaks when damping is high as the average can be significantly less than the initial peak drift of the cycle if the decay is rapid. Firstly, comparing the EVD calculated from the LDM (ξ_o) and the ALDM (ξ_{Ad}), it is clear that there is increased reliability and stability of the EVD response by eliminating the effect of even slight residual drifts. By comparing the EVD calculated from the ALDM (ξ_{Ad}) and the ALDEM ($\xi_{Ad-Energy}$), a decrease in EVD is shown at higher drifts but similar EVD is calculated at low drifts when the system is elastic and displacement peaks and energy peaks give the same result as with a linear system. The ALDEM results in lower EVD at high drifts when compared to ALDM due to the stiffness nonlinearity after uplift occurs. Use of LDM or ALDM for a nonlinear system will give inflated values of EVD due to the assumption of linear stiffness. This was proved in Twigden (2015) with a simple example. Based on these results it is believed that the energy method provides more realistic insight into the EVD of nonlinear systems as it accounts for the energy dissipated directly. Therefore ξ_o and ξ_{Ad} were not calculated or compared for the PreWEC wall systems.

The EVD was calculated using the ALDEM for each cycle and plotted against the corresponding average of the peak drifts of the respective cycle for SRW-A in Fig. 11(b) for both 1% and 2% snap back tests. For SRW-A, both the 1% and 2% drift tests showed a similar EVD trend with lower damping observed at higher displacements during the rocking phase of the decay and increased damping as the wall transitioned into the vibration phase within the stiffer portion of the force-displacement behaviour. The EVD for SRW-A was found to be 0.9% for displacements between 1.8-0.75% drift and increased up to 3.8% with decreasing drift. Also included in Fig. 11(b) is the EVD evaluated from the hysteretic area measured during a cyclic test on an identical wall (labelled SRW-B-CYCLIC) (Twigden *et al.* 2017). Interestingly much higher EVD was estimated from the cyclic test in comparison to the free vibration test, although a similar trend is observed with higher EVD at small amplitude cycles. The EVD variability was considered to be partially due to the increased damage in the wall toe that accumulated during the repeated reverse cyclic test compared to the snap back tests. However, the variability is also likely due to the method of EVD evaluation.

The EVD was calculated using the ALDEM and plotted against the corresponding average of the peak drifts of the respective cycle for all PreWEC systems and is presented in Fig. 12(a), (b), and (c). The highest EVD ratios calculated for PreWEC-A, B, and C at peak drifts of approximately 1% were 14.7%, 20.7%, and 25.8%, respectively. All three PreWEC walls showed increasing EVD with increasing lateral drift. PreWEC-A was expected to and had the lowest damping of the PreWEC walls as it had the lowest number of O-connectors per joint. PreWEC-C attained the highest amount of EVD due to the higher number of O-connectors

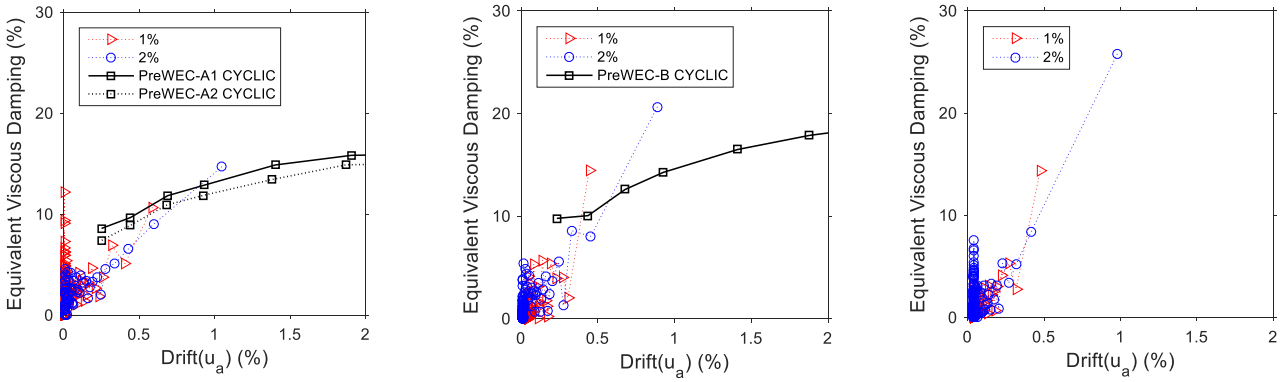

(a) (c) (e)

Fig. 12 PreWEC walls EVD, (a) PreWEC-A, (b) PreWEC-B, (c) PreWEC-C

per joint and the lower PT force. Also included in Fig. 12(a), and (b) is the EVD evaluated from cyclic tests on identical walls (Twigden *et al*. 2017) and labelled PreWEC-A1/2-CYCLIC and PreWEC-B-CYCLIC. For the two cyclic test comparisons the free vibration EVD was consistently higher at high drifts and lower at drifts below 0.75%. Although there was a significant difference between the magnitudes of EVD ratio between the two test methods a similar trend was observed. The higher EVD at higher drifts found for the PreWEC systems is likely due in part to the inclusion of contact damping, and also due to the different test and evaluation methods as previously stated. Higher damping was found from the cyclic tests at low drifts due to the concrete crushing and O-connector yielding that occurred as the drift levels were slowly increased, while for the snap back testing less cycles occurred at lower drifts and the concrete crushing and O-connector yielding would have been incorporated into the higher drift response and then occurred to a lesser degree at the lower drifts. The difference between the cyclic test EVD and the snap back test EVD is greater for the SRW shown in Fig. 11(b) than the two PreWEC walls shown in Fig. 12(a), and (b). This difference is attributed to the increased damage in the wall toe that accumulated during the SRW-A cyclic test as described above. This is more prominent for SRW-A due to the low damped nature of the system in comparison to the PreWEC systems.

8. Conclusions

An experimental investigation of the pseudo-static and dynamic properties of UPT concrete rocking walls was presented. One SRW and three PreWEC systems were subjected to snap back testing that included a monotonic pushover response and dynamic free vibration decay. During all tests the lateral load behaviour of the walls was consistent with their low-damage design philosophy, with rocking at the wall base and negligible damage was observed for all walls. In addition to examining the snap back test results, valuable comparisons were also made between the snap back tests and previously conducted reverse cyclic tests on identical walls that were reported elsewhere. As listed below a number of conclusions have been drawn based on the test observations and response comparisons:

- As expected SRW-A exhibited an approximately bi-linear response and the PreWEC walls showed increased strength and energy dissipation due to the addition of O-connectors. The inclusion of more O-connector dissipaters decreased the accelerations seen by the wall when comparing PreWEC systems of the same strength.
- The good alignment of the previously reported cyclic test lateral-load response with the pushover data and inertia force-displacement demonstrated the consistency in behaviour of UPT walls regardless of loading rate.
- Despite previous cyclic testing of identical wall specimens indicating significant residual drifts in the order of 0.1-0.4%, negligible residual drifts occurred during snap back tests on all walls regardless of the PT force and number of O-connectors.
- The fundamental frequency of all four wall systems was found to be significantly lower than that calculated using the gross section stiffness. This observation further confirmed the reduced stiffness observed during pseudo-static cyclic tests on identical wall. The proportion of the gross section moment of inertia required to attain the measured fundamental frequency was $0.48I_g$ for SRW-A and between $0.74\text{-}0.8I_g$ for the PreWEC walls.
- The local response parameters demonstrated that the dynamic behaviour of UPT wall systems is well represented by pseudo-static tests for parameters such as neutral axis and PT force, however higher strains in the compression toe of the wall can be expected due to toe impact during dynamic rocking.
- An adjusted logarithmic decrement energy method was used to evaluate the EVD of the wall systems. SRW-A was found to have EVD between 0.9-3.8%. PreWEC-A, B, and C were found to have maximum EVD ratios of 14.7%, 20.7%, and 25.8% respectively. The snap back test EVD results showed increased EVD at high drifts for all PreWEC walls and lower EVD at low drifts when compared to the cyclic test EVD. This is due to the nature of the loading and the influence of dynamic effects. However, for SRW-A higher EVD was calculated for the cyclic tests in comparison to the snap back tests due to the increased cycles and cumulative

damage.

Acknowledgments

Funding for this research was provided by the University of Auckland Engineering Faculty Research and Development Fund Project No. 3702479. Assistance provided by Alex Shegay, James King, Dan Ripley, and Mark Byrami was much appreciated. Collaboration with Professor Sri Sritharan from Iowa State University via the NEES Rocking Wall project (NSF-NEESR: 1041650) is also acknowledged.

References

Aaleti, S. and Sritharan, S. (2009), "A simplified analysis method for characterizing unbonded post-tensioned precast wall systems", *Eng. Struct.*, **31**(12), 2966-2975.

Abramson, D. (2013), "Comprehensive evaluation of multistrand post-tensioning anchorage systems for seismic resilient rocking wall structures", Master of Science, The University of Minnesota.

Belleri, A., Schoettler, M.J., Restrepo, J.I. and Fleischman, R.B. (2014), "Dynamic behavior of rocking and hybrid cantilever walls in a precast concrete building", *ACI Struct. J.*, **111**(3), 661-671.

Chopra, A.K. (2007), *Dynamics of Structures: Theory and Applications to Earthquake Engineering*, Prentice Hall, Upper Saddle River, NJ.

Galusha, J.G. (1999), "Precast, post-tensioned concrete walls designed to rock", M.S.C.E. Thesis, University of Washington.

Henry, R.S., Aaleti, S., Sritharan, S. and Ingham, J.M. (2010), "Concept and finite-element modeling of new steel shear connectors for self-centering wall Systems", *J. Eng. Mech.*, **136**(2), 220-229.

Henry, R.S., Brooke, N.J., Sritharan, S. and Ingham, J.M. (2012), "Defining concrete compressive strain in unbonded post-tensioned walls", *ACI Struct. J.*, **109**(1), 101-112.

Henry, R.S., Sritharan, S. and Ingham, J.M. (2016), "Finite element analysis of the PreWEC self-centering concrete wall system", *Eng. Struct.*, **115**, 28-41.

Henry, R.S., Sritharan, S. and Ingham, J.M. (2016), "Residual drift analyses of realistic self-centering concrete wall systems", *Earthq. Struct.*, **10**(2), 409-428.

Holden, T., Restrepo, J. and Mander, J.B. (2003), "Seismic performance of precast reinforced and prestressed concrete walls", *J. Struct. Eng.*, **129**(3), 286-296.

Kurama, Y. (2002), "Hybrid post-tensioned precast concrete walls for use in seismic regions", *PCI J.*, **47**(5), 36-59.

Kurama, Y.C., Sritharan, S., Fleischman, R.B., Restrepo, J.I., Henry, R.S., Cleland, N.M., Ghosh, S.K. and Bonelli, P. (2018), "Seismic-resistant precast concrete structures: State of the art", *J. Struct. Eng.*, **144**(4), 03118001.

Mander, J.B., Priestley, M.J.N. and Park, R. (1988), "Theoretical stress-strain model for confined concrete", *J. Struct. Eng.*, **114**(8), 1804-1826.

Marriott, D. (2009), "The development of high-performance post-tensioned rocking systems for the seismic design of structures", Doctor of Philosophy, PhD Thesis, University of Canterbury, Christchurch.

Marriott, D., Pampanin, S., Bull, D. and Palermo, A. (2008), "Dynamic testing of precast, post-tensioned rocking wall systems with alternative dissipating solutions", *Bull. NZ Soc. Earthq. Eng.*, **41**(2), 90-103.

Nagae, T., Matsumori, T., Shiohara, H., Kabeyasawa, T., Kono, S., Nishiyama, M., Moehle, J., Wallace, J., Sause, R. and Ghannoum, W. (2014), "The 2010 E-defense shaking table test on four-story reinforced concrete and post-tensioned concrete buildings", *Proceedings of the NCEE 2014 - 10th U.S. National Conference on Earthquake Engineering: Frontiers of Earthquake Engineering*.

Nazari, M., Sritharan, S. and Aaleti, S. (2017), "Single precast concrete rocking walls as earthquake force-resisting elements", *Earthq. Eng. Struct. Dyn.*, **46**(5), 753-769.

NZS 3101:2006 (2006), Concrete Structures Standard, Standards New Zealand, Wellington, New Zealand.

Perez, F.J., Pessiki, S. and Sause, R. (2013), "Experimental lateral load response of unbonded post-tensioned precast concrete walls", *ACI Struct. J.*, **110**(6), 1045-1055.

Priestley, M.J.N., Sritharan, S.S., Conley, J.R. and Pampanin, S. (1999), "Preliminary results and conclusions from the PRESSS five-story precast concrete test building", *PCI J.*, **44**(6), 42-67.

Sritharan, S., Aaleti, S. and Thomas, D.J. (2007), "Seismic analysis and design of precast concrete jointed wall systems", ISU-ERI-Ames Report ERI-07404, Department of Civil, Construction and Environmental Engineering, Iowa State University, Ames, IA.

Sritharan, S., Aaleti, S., Henry, R.S., Liu, K.Y. and Tsai, K.C. (2015), "Precast concrete wall with end columns (PreWEC) for earthquake resistant design", *Earthq. Eng. Struct. Dyn.*, **44**(12), 2075-2092.

Twigden, K.M. (2015), "Dynamic response of unbonded post-tensioned rocking walls", Doctor of Philosophy, PhD Thesis, University of Auckland, Auckland.

Twigden, K.M. and Henry, R.S. (2015), "Experimental response and design of O-connectors for rocking wall systems", *Struct.*, **3**, 261-271.

Twigden, K.M., Sritharan, S. and Henry, R.S. (2017), "Cyclic testing of unbonded post-tensioned concrete wall systems with and without supplemental damping", *Eng. Struct.*, **140**, 406-420.

Walsh, K.Q. and Kurama, Y.C. (2010), "Behavior of unbonded post-tensioning monostrand anchorage systems under monotonic tensile loading", *PCI J.*, **55**(1), 97-117.

Wight, G.D., Ingham, J.M. and Kowalsky, M.J. (2006), "Shaketable testing of rectangular post-tensioned concrete masonry walls", *ACI Struct. J.*, **103**(4), 587-595.

KT